AD-A095 691 NATIONAL BUREAU OF STANDARDS WASHINGTON DC CENTER FOR--ETC F/G 21/2
IGNITION OF A LIQUID FUEL UNDER HIGH INTENSITY RADIATION.(U)
NOV 80 T KASHIWAGI, T J OHLEWILLER AFOSR-ISSA-80-0010

UNCLASSIFIED AFOSR-TR-81-0111 NL

END
DATE FILMED
3-81
DTIC

Unclassified

REPORT DOCUMENTATION PAGE

READ INSTRUCTIONS BEFORE COMPLETING FORM

1. REPORT NUMBER	2. GOV ACCESSION NO.	3. RECIPIENT'S CATALOG NUMBER
AFOSR-TR- 81-0111	AD-A095691	

4. TITLE (and Subtitle)
Ignition of a Liquid Fuel Under High Intensity Radiation

5. TYPE OF REPORT & PERIOD COVERED
Interim
October 1, 1979-September 30, 1980

6. PERFORMING ORG. REPORT NUMBER

7. AUTHOR(s)
Takashi Kashiwagi
Thomas J. Ohlemiller

8. CONTRACT OR GRANT NUMBER(s)
AFOSR-ISSA-80-00010

9. PERFORMING ORGANIZATION NAME AND ADDRESS
Center for Fire Research
National Bureau of Standards
Washington, D.C. 20234

10. PROGRAM ELEMENT, PROJECT, TASK AREA & WORK UNIT NUMBERS
61102F
2308/A2

11. CONTROLLING OFFICE NAME AND ADDRESS
Air Force Office of Scientific Research/NA
Building 410
Washington, D.C. 20332

12. REPORT DATE
November 1980

13. NUMBER OF PAGES
25

14. MONITORING AGENCY NAME & ADDRESS(if different from Controlling Office)

15. SECURITY CLASS. (of this report)
Unclassified

15a. DECLASSIFICATION/DOWNGRADING SCHEDULE

16. DISTRIBUTION STATEMENT (of this Report)

17. DISTRIBUTION STATEMENT (of the abstract entered in Block 20, if different from Report)
Approved for public release; distribution unlimited.

18. SUPPLEMENTARY NOTES

19. KEY WORDS (Continue on reverse side if necessary and identify by block number)
Radiative Ignition Mechanism
Aircraft Fuel Ignition
Laser Supported Ignition

20. ABSTRACT (Continue on reverse side if necessary and identify by block number)
The time sequence of behavior of liquid fuel and of the fuel vapor near the liquid surface during the laser-induced ignition period was observed by high speed schlieren and direct photography. A CW carbon dioxide laser with fluxes up to 2500 watts per square centimeter was used; beam incident angles were 30 and 90 degrees with respect to the liquid surface. Both n-decane and 1-decene were used as the liquid fuel. The pictures reveal, in time sequence, the formation of a radial wave, a central surface depression, bubble nucleation/ growth/bursting followed by complex surface →

DD FORM 1 JAN 73 1473 EDITION OF 1 NOV 65 IS OBSOLETE

Unclassified
SECURITY CLASSIFICATION OF THIS PAGE (When Data Entered)

Unclassified

motion and further bubbling; typically several (or many) bubble cycles preceded ignition. Effects of laser flux level, incident laser angle and absorption coefficient of the liquid on the formation of bubbles, the size of bubbles, the frequency of bubble formation and the vaporization process are studied. A feasibility study of the use of two-wavelength holographic interferometry to measure vapor concentration and its temperature during the ignition period has been undertaken. The design of a system to measure infrared absorption coefficients of liquid vapor at elevated temperatures was completed.

Unclassified

SECURITY CLASSIFICATION OF THIS PAGE (When Data Entered)

Ignition of a Liquid Fuel Under High Intensity Radiation

Annual Progress Report for October 1, 1979 to September 30, 1980

Takashi Kashiwagi
Thomas J. Ohlemiller
Center for Fire Research
National Bureau of Standards
Washington, D.C. 20234

This work is supported by the Air Force Office of Scientific Research
Under Contract AFOSR-ISSA-80-00010.

1. Objectives and Work Statement

Laser technology has been rapidly advancing in the last two decades. Power outputs of modern lasers have increased significantly and these lasers can now be used as tactical weapons. A high power laser weapon can ignite aircraft fuel after fuel tank penetration and can thus cause a fire or explosion on the aircraft. To increase aircraft survivability against such weapons, one of the most effective safeguards is the prevention of ignition. However, the ignition of flammable liquids by laser radiation has been little studied and is poorly understood. The objective of this study is to obtain a fundamental understanding of the mechanism of ignition of flammable liquids by a high power laser.

In the previous study by one of the authors, two important phenomena were observed: (1) the appearance of first flaming in the gas phase and (2) complex liquid behavior, such as bubbling, near the surface during the ignition delay period. These indicate that ignition is caused by absorption of the incident laser energy by fuel vapor in the gas phase and that the build-up of the fuel vapor may be controlled by the complex liquid behavior. To understand these mechanisms more clearly and quantify them for use in future theoretical models, the following three topics are being examined in the current three year study period: (1) detailed observation of the behavior of the liquid fuel near the surface, (2) measurement of absorption coefficients of fuel vapors at elevated temperatures and (3) measurement of distributions of fuel vapor concentration of and temperature in the gas phase during the ignition period.

This report summarizes the progress and output from each of the above topics during the first year of the planned three year period.

2. Status of the Research Effort

The current status of each of the above topics is described here:

(1) Observation of liquid behavior near the surface.

The first phase of this work is complete; it is reported on in the Appendix. The time sequence of the behavior of the liquid fuel and of the fuel vapor near the liquid surface was observed by high speed photography. Two high speed cameras were used simultaneously in each experiment. One of them photographed the liquid surface behavior from the top. The second camera photographed either the behavior of fuel vapors in the gas phase made visible by a schlieren system or the behavior of the liquid beneath the surface by direct photography. A CW CO_2 laser with fluxes up to 2500 W/cm^2 was used with beam incident angles of 30 and 90 degrees with respect to the liquid surface. Both n-decane and 1-decene were used as the liquid fuel. The pictures reveal, in time sequence, the formation of a radial wave, a central surface depression, bubble nucleation/growth/bursting followed by complex surface motion and further bubbling. Effects of laser flux level, incident laser angle and absorption coefficient of the liquid (16 cm^{-1} and 50 cm^{-1}) on the formation of bubbles, the size of the bubbles, the frequency of bubble formation and the vaporization process were studied. A simple order of magnitude analysis is applied to ascertain the dominant processes that underly these phenomena. Results are discussed in detail in the Appendix.

(2) Measurement of infrared absorption coefficients of fuel vapors at elevated temperatures.

The design of the experimental set up is completed and its schematic illustration is included in this report. A small black-body will be used as a radiation source; its temperature can be well controlled up to 1300 K. The heated sample cell is 5 cm in inside diameter and 15 cm long with two BaF windows on the ends. Its temperature is well controlled up to 1000 K. The cell with the heater is currently under construction and its completion is expected within the next few months. The infrared monochrometer, a stepping motor assembly for driving the grating and a desk top computer for overall control are currently available. The programing and the interfacing between the computer and the monochrometer will start shortly. The system will measure absorption coefficients of fuel vapors from 2.0 to 11 μm. The total path length from the exit of the black body to the entrance of the monochrometer is about 180 cm. To avoid the effect of absorption by water vapor in the room air, most of the optical path will be enclosed and purged by dry nitrogen.

(3) Measurement of distribution of fuel vapor concentration and temperature during the ignition period.

We have undertaken a feasibility study of the use of holographic interferometry. Since refractive index is a function of species concentration and temperature, two different wavelengths need to be used to obtain both quantities. As a first step, a single wavelength holographic interferometry system using a He-Ne laser has been set up to assess the technique and the preliminary results are described in the Appendix. At present, the second wavelength from an Ar-ion laser (488 nm) is being added to the system and its schematic illustration is included in this report. A photograph of the system is also included in this report. Final adjustment of the system is in progress and a preliminary study taking high speed holographic interferometer movies during the ignition period will begin in the near future.

3. Cumulative list of publications

1. Kashiwagi, T., "Ignition of a Liquid Fuel Under High Intensity Radiation," Comb. Sci. Tech., Vol. 21, 1980, pp. 131-139.

2. Kashiwagi, T., Baum, H.R., and Rockett, J.A., "Ignition of Liquid Fuel Under High Intensity Radiation." AFOSR-TR-80-0476, January, 1980.

3. Kashiwagi, Takashi, Ohlemiller, T.J., and Kashiwagi, Takao, "Ignition Mechanism of a Liquid Fuel by High Intensity Radiation," AIAA preprint number 81-0180, AIAA 19th Aerospace Sciences Meeting. This will probably be submitted to Combustion and Flame.

4. Kashiwagi, T., "Effects of Sample Orientation on Radiative Ignition." Submitted to Combustion and Flame.

4. Interactions

One of the authors (T. Kashiwagi) has had several discussions with Mr. Jon Manheim, Wright Patterson Air Force Laboratories, about the observations on the liquid behavior near the liquid surface during the ignition period.

5. Appendix

Attached is a copy of the preprint, AIAA-81-0180, for the 19th Aerospace Sciences meeting, St. Louis, January, 1981.

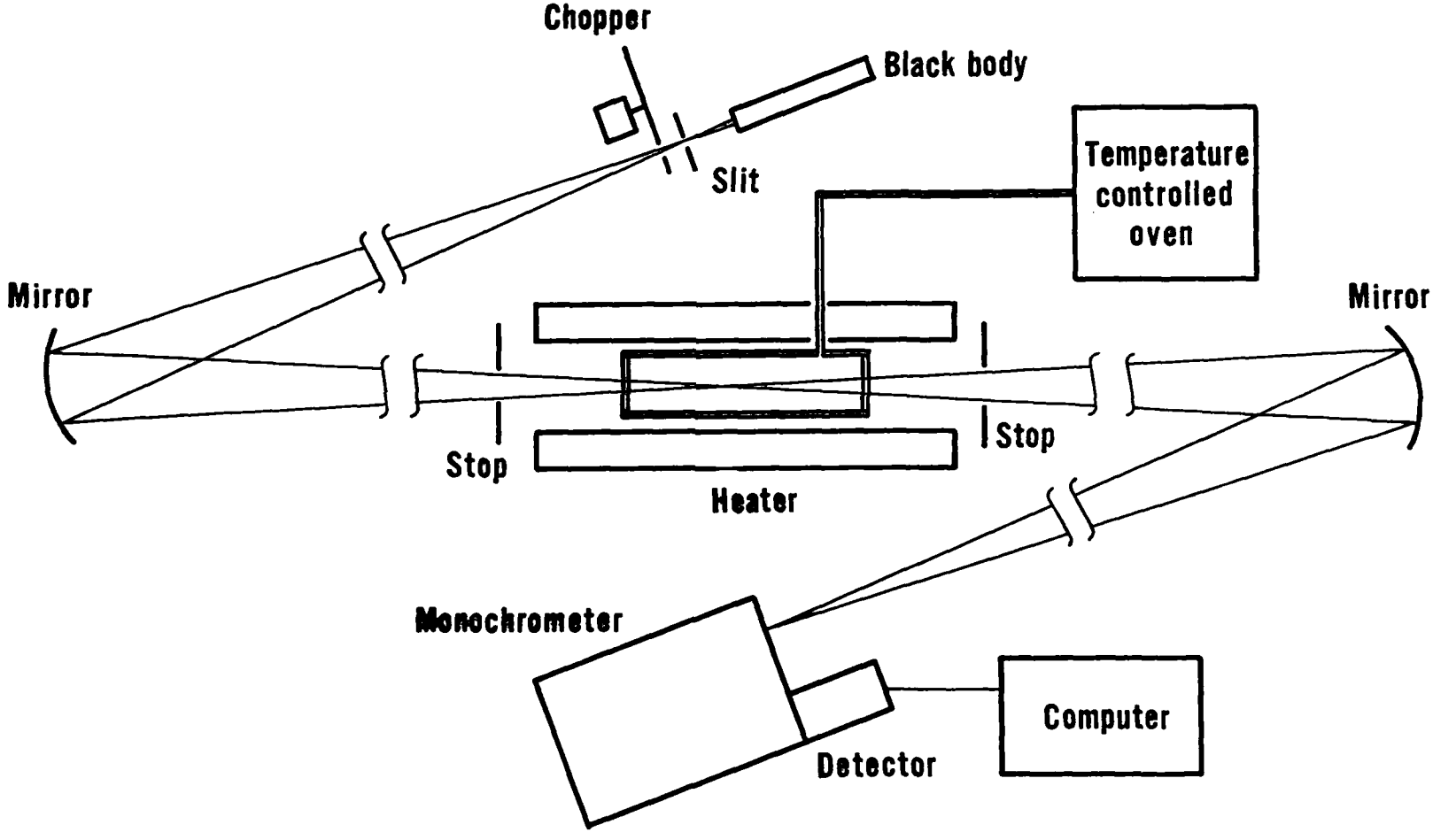

SCHEMATIC ILLUSTRATION OF IR ABSORPTION MEASUREMENT APPARATUS AT ELEVATED TEMPERATURES

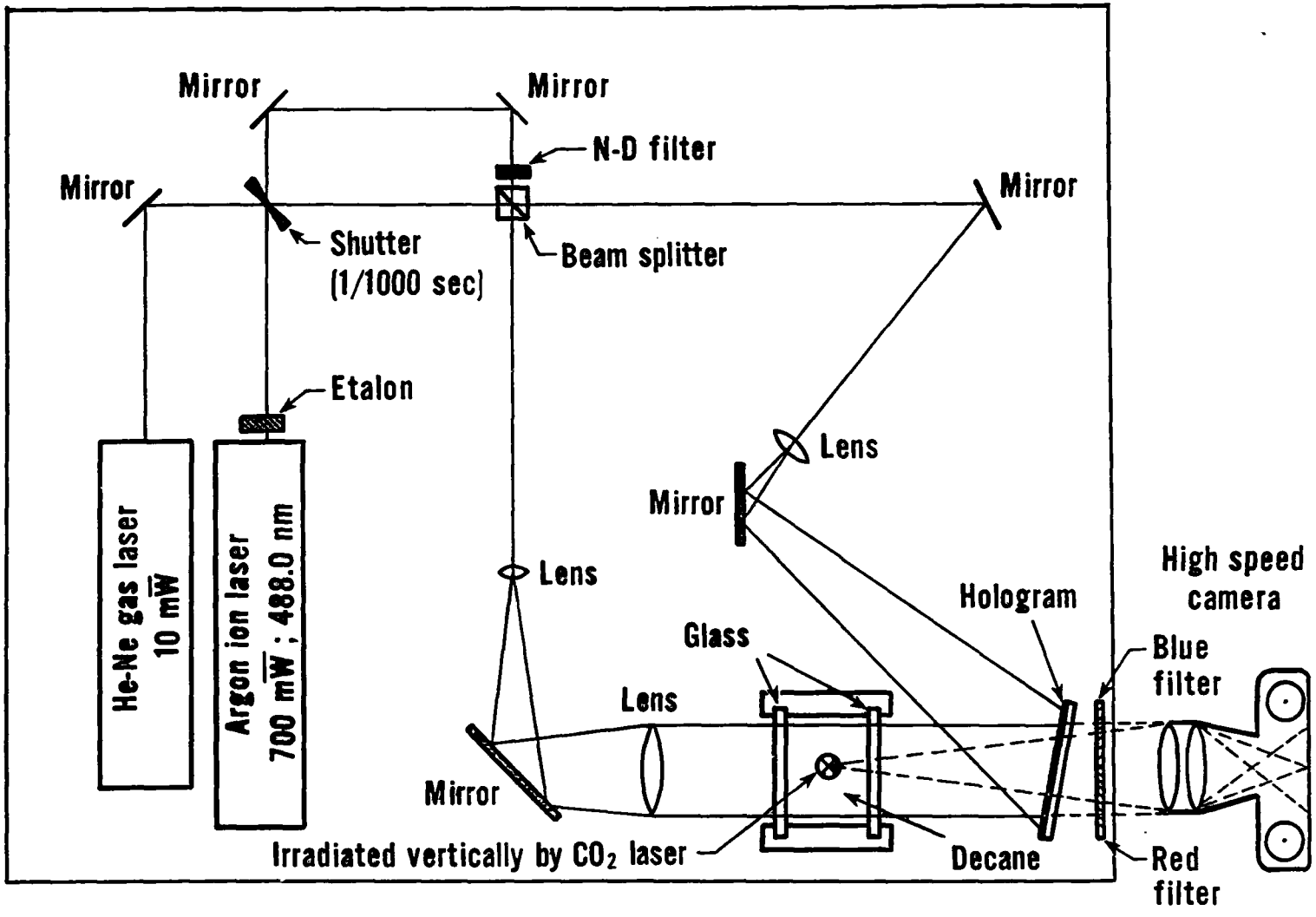

SCHEMATIC ILLUSTRATION OF TWO - WAVELENGTH HOLOGRAPHIC INTERFEROMETER APPARATUS

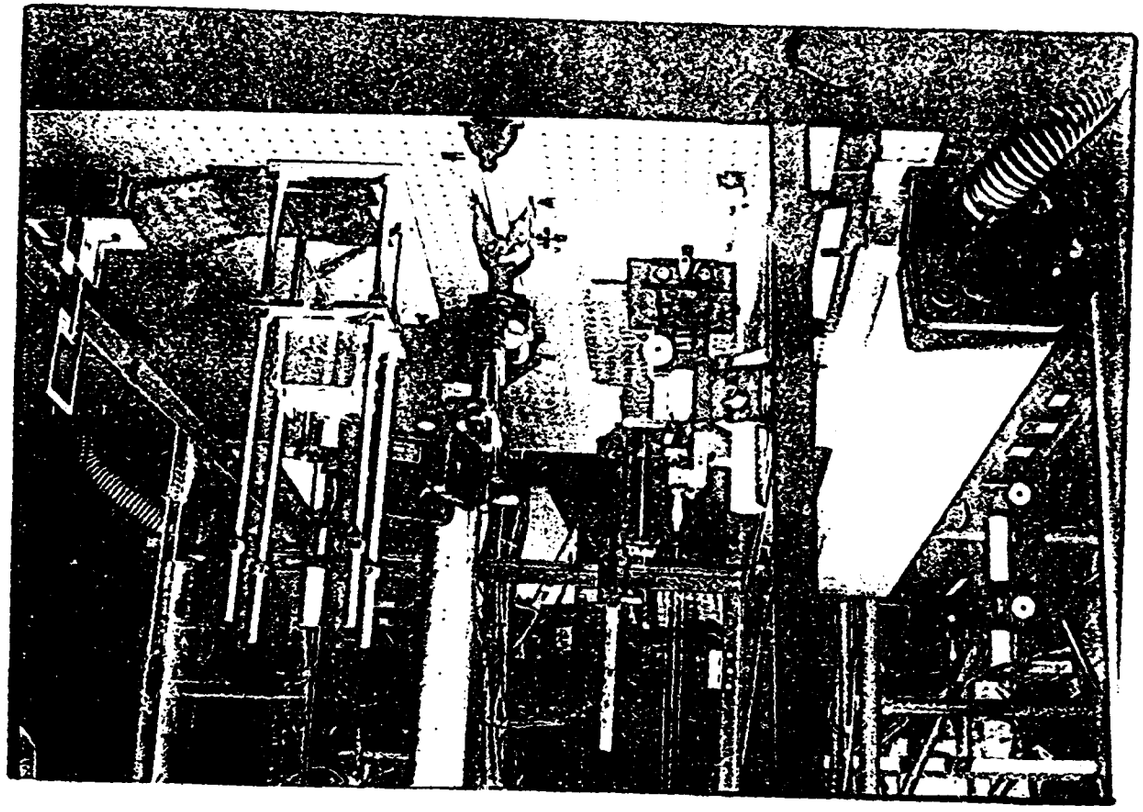

IGNITION MECHANISM OF A LIQUID FUEL BY HIGH INTENSITY RADIATION

Takashi Kashiwagi*, T. J. Ohlemiller** and Takao Kashiwagi+
National Bureau of Standards
Washington, D.C. 20234

Abstract

As an aid to understanding the ignition mechanism of liquid fuels under high intensity radiation, the time sequence of behavior of the liquid fuel and of the fuel vapor near the liquid surface was observed by high speed schlieren and direct photography. A CW CO_2 laser with fluxes up to 1000 W/cm^2 was used with beam incident angles of 30 and 90 degrees with respect to the liquid surface. Both n-decane and 1-decene were used as the liquid fuel. The pictures reveal, in time sequence, the formation of a radial wave, a central surface depression, bubble nucleation/growth/bursting followed by complex surface motion and further bubbling. Effects of laser flux level, incident laser angle and absorption coefficient of the liquid (16 cm^{-1} and 50 cm^{-1}) on the formation of bubbles, the size of the bubbles, the frequency of bubble formation and the vaporization process were studied. A simple order of magnitude analysis is applied to ascertain the dominant processes that underly these phenomena.

1. Introduction

Laser technology has been rapidly advancing in the last two decades. Power outputs of modern lasers have increased significantly and these lasers can now be used as tactical weapons. A high power laser weapon can ignite aircraft fuel after fuel tank penetration and can thus cause a fire or explosion on the aircraft. To increase aircraft survivability against such weapons, one of the most effective safeguards is the prevention of ignition. However, the ignition of flammable liquids by laser radiation has been little studied and is poorly understood, although the ignition of solids (1,2) and vaporization of liquid droplets by high power lasers (3,4) has been studied.

In previous studies (5,6) by one of the authors, the change in ignition delay time for a liquid fuel was measured for varying CO_2 laser flux, laser incident angle and the size of the liquid container. This work clearly showed the ultimate development of thermal runaway (ignition) in the gas phase as a consequence of laser energy absorption by the fuel vapors there. However, further understanding of the behavior of the vaporizing liquid and its coupling to the build-up of vapor in the gas phase during the ignition period is needed as a prelude to developing a theoretical model that could aid in avoiding ignition.

The objective of the present study is to obtain an increased understanding of the mechanism of ignition by observing with various photographic techniques the sequence of events at the liquid surface and in the gas phase near the surface during the ignition delay period. This paper reports various photographic observations on n-decane and n-decene during laser irradiation and describes the formation, growth and collapse of bubbles in the liquid and the growth of a vapor plume in the gas. The primary physical processes in the overall behavior are deduced from these observations by simple qualitative and order of magnitude analyses.

2. Experimental Apparatus

A schematic illustration of the experimental apparatus is provided in Figure 1. A Coherent Radiation Model 41 CO_2 laser* emits an approximately 6-7 mm diameter beam. Beam power was varied from 195 to 340 watts in the fundamental mode which has a nearly Gaussian power distribution across the beam. The incident flux distribution at the sample surface position is measured prior to an experiment by traversing a water cooled, horizontally-mounted calorimeter with 0.25 mm diameter sensing element. The maximum value of the incident flux measured in this manner is that reported as the incident radiant flux in this study.

A rotating mirror is used as a shutter to provide a step-function onset of irradiance; it then remains open through the ignition event. The onset of laser irradiation, i.e. t=0, was determined by the signal from a sensitive pyroelectric detector collecting part of the laser beam scattered from a mirror. The signal change turned off a neon lamp inside the high speed camera as an event mark on the film through electronic switching circuitry. However, comparison of this event mark with the onset of events on corresponding picture frames indicated and caused some ambiguity in quantifying precisely each sequence in terms of time from the onset of the laser irradiation. Consequently, timing was frequently referenced to the onset of a surface wave believed to result from photon pressure, as described below. Further improvements in procedures to determine the start of the experiment are necessary in future studies.

Two high speed cameras (HYCAM) were used simultaneously in each experiment. One of them photographed the liquid surface behavior from the top. The camera was focused on the surface and mounted as shown in Figure 1 so that the illumination seen by this camera was specularly reflected light from an approximately 10 cm high diffusing screen illuminated in turn by a tungsten-halogen lamp. This illumination technique provides graded but high contrast for detecting changes in surface inclination. The second camera photographed either the behavior of fuel vapors in the gas phase made visible by a schlieren system as shown in Figure 1

---

*Materials Engineer, Member AIAA

**Research Engineer

+On leave from Tokyo Institute of Technology

*In order to adequately describe materials and experimental procedures it is occasionally necessary to identify commercial products by manufacturer's name or label. In no instance does such identification imply endorsement by the National Bureau of Standards nor does it imply that the particular product or equipment is necessarily the best available for that purpose.

or the behavior of the liquid beneath the surface by direct photography. In schlieren photography, the He-Ne laser beam was cut horizontally from the bottom by a knife edge. Kodak 4X negative film for high speed photography was used for all pictures in this study; most prints were made at enhanced contrast.

The dimensions of the liquid container are 5.5 cm x 7.8 cm by 5.5 cm deep. These dimensions are large enough so as not to affect the ignition delay time (5). Two optical grade quartz flats were used as observation windows in two sides of the container. The container was filled to the top with the liquid fuel.

Ignition is defined by the first light emission detected by a photomultiplier (S-5 response), the output of which is recorded by an oscillographic recorder with maximum resolution of $\pm$ 1 msec. At the onset of flaming, a step-function-like output of the photomultiplier is obtained. This provides an unambiguous measure of the time of ignition. In this study, n-decane and 1-decene were used as the liquid fuels and air as the environmental gas. The two fuels were chosen to be as similar as possible in all properties except absorptivity with respect to the CO_2 laser radiation; 1-decene has a substantially higher effective absorptivity (approximately 50 cm^{-1} vs. 16 cm^{-1}) in the liquid and probably also in the vapor as well.

3. Results and Discussion

Range of Laser Flux

In the authors' previous study (5,6) using decane, the range of laser fluxes was up to 4000 W/cm^2 and ignition delay time was in the range of 0.06~1.0 sec. Since the objective of the present study is detailed observation of behavior of the liquid and of vapor build-up in the gas phase, low laser fluxes in the range of 350 - 950 W/cm^2 were used to make the behavior slow enough to be more easily observed. Also, decene was added as a second liquid fuel to examine the effect of absorption coefficient on the overall behavior. With the present conditions, ignition delay times of decane are in the range of 0.35~1.0 sec and those of decene, 0.040~0.085 sec.

Parametric Study of Phenomena

Three parameters, laser flux, incident laser angle with respect to the liquid surface and absorption coefficient of the liquid, were selected in this study. Top view and side view pictures were taken with various combinations of these parameters. Typical examples are shown in this paper. Pictures of decane are shown in Figure 2 for an incident laser flux of 730 W/cm^2 and in Figure 3a and 3b for 360 W/cm^2. The dark band in the side view pictures is due to the liquid meniscus at the window of the container. Surface behavior as seen from above and formation of the vapor cloud in the gas phase as seen from the side are shown for decane with an incident laser angle of 30°. In Figure 2, the top view pictures and side view schlieren pictures are shown side by side in correlated time sequence. The left columns of pictures are of the top view and the right columns are of the side view. For the low laser flux case, top view pictures are shown in Fig. 3a and side view schlieren pictures in Fig. 3b. In Figures 3a and 3b, the correlation between the top view pictures and the side view schlieren pictures is not well established due to the lack of a precise determination of the time when the laser starts to irradiate the decane surface, as described in the previous section (and differences in camera framing rates, as well). The top view pictures in both figures indicate the formation of a faint ring-shape wave motion moving slowly outward radially. As time increases after the laser irradiation begins, the shape of the ring becomes clearer; the center part of the ring is concave. With further increases in time, the top view pictures show a further surface depression at the center of the ring. This further depression is circular and its diameter is about the same as that of the incident laser beam. At the same time, the pictures at low flux indicate the development of small scale complex wave motions between the area of the further depression and the ring. In Fig. 3b, side view schlieren pictures show the formation and growth of a laminar plume-like cloud of decane vapor. Decane, with its high molecular weight (142), is heavier than the surrounding air despite its elevated temperature (boiling point 174°C). The formation and the growth of the vapor plume is thus due to the momentum implicit in the jet-like, rapid vaporization of decane instead of to buoyancy. Therefore, it is probable that the further central surface depression and the subsequent small wavy motions are caused by this momentum (see below). In Figure 2, side view schlieren pictures corresponding to the appearance of the further central depression do not show any laminar plume-like cloud. (Note that it has much less time to move up from the surface.) This is probably due to a low sensitivity setting of the schlieren system for Figure 2. The amount of knife edge cutting could not be set the same for all schlieren photographs. Further discussion of this early sequence of events is given later.

In Figure 2, shortly after the appearance of the further central surface depression, a black circle appears in the center of the ring. A similar black circle also appears much later in Fig. 3a. The corresponding side view schlieren picture in Fig. 2 indicates a sudden release of decane vapor into the gas phase. The black circle becomes larger with time and the vaporization of decane becomes more extensive and turbulent. Side view direct close-up pictures of decane near the surface, shown in Figure 4, indicate an extremely rapid growth of a bubble (its diameter is approximately 3 mm) beneath the surface. These pictures were taken with different conditions from those of Figs. 2 and 3; they are for decane, a laser incident angle of 30° from right to left and a laser flux of about 2600 W/cm^2. Some properly lighted sequences of top photos clearly show that even at much lower fluxes than this the bubble bursts as quickly as it forms; therefore, the observed black circle in Figs. 2 and 3 is an open hole left by the bubble. Shortly after the bubble reaches its maximum size it starts to shrink; this is made complicated by the appearance of a second smaller bubble in the side wall of the first as shown in Fig. 4 (a high flux phenomenon; see below). The decane surface becomes very complex and, except at low fluxes, a second bubble forms before these complex motions damp out. Thus the cycle of formation and collapse of a bubble sandwiched between periods of no bubble is repeated; however, the frequency of bubbling is not exactly regular. The top view pictures in Fig. 2 and

Fig. 3a indicate the formation and radial outward movement of waves apparently generated by rapid bubble formation/collapse and the associated violent vaporization process. These waves interact with the previously generated waves so that the surface structure becomes extremely complex as shown in the last columns of Figure 2. At the same time, the side view schlieren pictures indicate violent vaporization, with decane vapor and liquid decane droplets being thrown in all directions.

Gas phase ignition generally occurs during this complex behavior in the liquid and gas phase. The onset of ignition is controlled by the amount of vapor, the degree of mixing of vapor with air and the amount of absorption of the laser energy by the vapor. This is illustrated in Fig. 5 which shows the location of the first appearance of flame with respect to the irradiated area. In this figure, a side view of the decane surface is seen through the window; the surface is the broad horizontal line across each frame (broadened by the meniscus at the window). The upper part of each frame shows the gas phase; the lower part is liquid decane. The incident laser beam comes from left to right at an angle of 30 degrees with respect to the surface. The small white area of flame that first appears in the bottom of the second column of frames is clearly seen to be in the gas phase about 1 cm above the surface and about 2 cm to the left of the irradiated area (indicated by the bubble on the right side of the pictures). The flame spreads upward from the point of its first appearance, presumably assisted by buoyancy, and then spreads toward the irradiated area of the decane surface along the laser beam.

The observed effects of three parameters, laser flux, incident laser angle and the value of absorption coefficient of the liquid, on the behavior of the liquid surface, bubble formation and vaporization are summarized in Table 1. All information except ignition delay times was obtained from a total of twenty eight separate movies. Since the onset of the laser irradiation is not precisely defined in these pictures and also since some of the phenomena are not sharply visible in some movies, values listed in this table may not be exact but they are sufficiently so for the objectives of this paper.

Laser Flux

Higher laser flux shortens the time to the first appearance of the central surface depression associated with the momentum of the laminar vaporization plume and to the appearance of the first bubble. This is clearly demonstrated by comparison of pictures shown in Figs. 2 and 3. The frequency of the bubble formation/collapse cycle tends to increase with increases in laser flux. It also appears qualitatively that the laser flux does not have a significant effect on the size of the bubbles. The pictures show that higher laser flux causes the behavior of the liquid surface to become complex earlier and vaporization tends to become more vigorous.

Laser Incident Angle

Top and side view pictures show that the qualitative behavior of the liquid phase at incident laser angles of 30 and 90 degrees does not differ significantly regardless of total laser power level. Any differences are caused mainly by the change in the laser flux due to the change in the irradiated area with the incident angle. One noticeable difference between the two angles occurs at high fluxes after the first bubble bursts but before it has collapsed. As was noted previously, in such high flux cases a second bubble can start to form in the wall of the first bubble and this complicates the collapse of the first. As shown in Fig. 4, the left side of the original bubble develops a bulge with the incident laser angle of 30 degrees from right to left. At 90 degrees, the bottom part of the original bubble shows this bulge.

Since ignition occurs at the location where the incident laser beam interacts with the appropriate mixture of fuel vapor and air, the location of the first appearance of the flame is expected to change with the incident laser angle. (This has not yet been checked experimentally). This idea is supported by the fact that, once bubbling starts, fuel vapor is thrown into the gas phase over almost the entire hemisphere by the violent vaporization process and not into a specific direction dependent on the incident laser angle.

Absorption Coefficient of Liquid

The effect of the value of the laser radiation absorption coefficient of the liquid on liquid behavior during the ignition period and also on the overall ignition delay was studied by a comparison of high speed pictures and the measured ignition delay time with decane and decene. The value of the absorption coefficient of decane with respect to the CO_2 laser is 16 cm^{-1} (6) and that of decene is about 50 cm^{-1} (7). Since the only difference between the two molecules is one carbon-carbon double bond at the end of the carbon backbone for decene instead of all carbon-carbon single bonds for decane, the physical and chemical characteristics of the two liquids are close to each other; the normal boiling temperature of decane is 174.1°C versus 170.5°C for decene (8); the difference in molecular weight is two; thermal properties should be close to each other. Oxidation characteristics are expected to be quite similar, judging from the analogous pair, pentane and pentene. Flammability limits for pentane are 1.4 - 7.8% fuel in air; for pentene they are 1.65 - 7.7% fuel in air (9). Therefore, the difference between the two liquids for this study is mainly the difference in the value of absorption coefficient. Also, it is expected that a similar difference in absorption coefficient applies to vapors from the two liquids.

Top view pictures of decene during the ignition period are shown in Figure 6. The sequence of phenomena, i.e., circular wave motion, the central depression, bubble formation and complicated surface motion, is virtually the same as that of decane as seen in Figs. 2 and 3. The distinctive difference between pictures with decene and decane is the much shorter time scale of events with decene compared to that of decane. This is also indicated quantitatively in Table I in a comparison of various times for the same experimental conditions. It is interesting to note that the times to the appearance of the central depression and to the appearance of the first bubble for decene are about a factor of two to four shorter than those for decane. However, ignition delay times for decene are at least one order of magnitude shorter than those for decane. This indicates that the differences in absorption

coefficient between the liquids and the vapors both have a major effect on ignition delay time.

Other differences between the two liquids are the size of the bubbles and the bubble frequency. Bubbles for decene tend to be smaller than those for decane as shown in Table I, although the quantitative difference needs further definition. Also, bubble frequency for decene tends to be higher than that for decane under the same experimental conditions.

Sequence of Phenomena and Underlying Processes

Idealized Sequence. Figure 7 shows a series of sketches, in cross-section, of what are believed to be the major steps in the radiation-induced vaporization process. The starting condition, for the first bubble only, is a quiescent liquid at uniform temperature (room temperature). Recall that the incident beam profile is roughly Gaussian and therefore is strongly peaked in the center.

In the second sketch of Fig. 7, two changes are apparent. A wave is spreading outward radially from the locus of the beam center and the temperature for some depth below the surface has increased. The expected depth of the thermal wave will be examined more closely below. It is probable that the radial surface wave is due at least in part to photon pressure that suddenly exerts a sustained force on the surface. The static depth of a depression in the liquid surface induced by photon pressure is calculated by equating the static liquid head to the rate of momentum loss of the photons; the result is

$$h_p = (F/c\rho_L g)$$

where F is the photon energy flux, c is the speed of light, g is the acceleration due to gravity and ρ_L is the liquid density. For a peak radiant flux of the order of 1000 Watts/cm^2 (high end of current tests), the value of h_p is about 5 micrometers. As a static depression extending smoothly over the beam diameter, this would probably not be visible, even with the rather high contrast specular surface lighting used here. However, we have a dynamic situation here in which we view the surface response to the sudden onset of a force; this produces a wave whose steep sides contribute to its visibility. An additional contribution to this early wave may come from the transient volumetric expansion of the liquid as it heats. Decane expands about 10% in heating up 100°C; this would cause a static surface height increase of about 10% of the radiation absorption depth over the heating time and a radial outward displacement over the same interval of about 10% of the beam diameter. This may be more visible than the direct photon pressure effect. The identification of the wave with these early effects is important because, as was noted, the wave onset has been used as a zero time reference in several tests.

The wave speed is of the order of a few tens of centimeters per second but the exact value appears to vary in a manner not fully understood at present.

In the third sketch of Fig. 7, the surface has reached a sufficient temperature for vaporization to become appreciable. This vapor flux is visible as the laminar plume in some of the [illegible] photographs (e.g., Fig. 3b). This vapor absorbs some of the incoming radiation as will be discussed below. If the speed of this plume is sufficient, the reaction force against the surface can cause a further depression. Balancing the static and dynamic heads gives, for this surface depression,

$$h_R = \frac{\rho v_p^2}{2\rho_L g}$$

For an upward vapor plume speed of 75 cm/sec (roughly that obtained from Fig. 3b), one finds h_R is about 150 microns. A central depression is frequently visible in the top surface photographs for varying periods before the first bubble appears.

In cases where this depression (plus that due to photon pressure) persists for an extended period (tens of milliseconds) prior to bubble formation, it appears that some instability exists that causes small wavelenth surface waves to grow in amplitude especially around the periphery of the depressio... This may be a result of some coupling between wave-induced fluid motion, the vapor flux (which causes the waves) and the highly non-uniform radiant flux profile on the liquid surface.

In the fourth sketch of Fig. 7, the upper surface of the liquid has achieved appreciable super-heating because the preceding vaporization process from the top surface has not been able to remove a sufficient fraction of the incoming radiant energy. In the next sketch, this superheating results in bubble nucleation. The amount of superheating that occurs prior to nucleation will depend on the radiant flux, absorption coefficient of liquid, and on the purity of the liquid. In the absence of foreign nuclei for bubble formation, the higher radiant fluxes used here should be capable of pushing the liquid very near the superheat limit for the fuel. The superheat limit is set by thermodynamic considerations but its approach is typically constrained by the kinetics of homogeneous bubble nucleation and growth (10,11). The value is typically around 0.9 of the critical temperature; for decane this translates to 285°C (12). Since the normal (1 atm) boiling point of decane is 174°C, this means that one could, under the proper conditions, exceed the boiling point by 111°C before achieving homogeneous nucleation. Decene, whose boiling point is 170.5°C, should behave quite similarly since octane and octene do so (12).

In the present experiments, no special precautions were taken to assure the absence of potential nuclei in the fuels although in nearly all tests the fuels were clean enough to exhibit practically no scattering of the He/Ne laser light used in the schlieren photography. Ref. 13 gives a simple expression relating degrees of superheating to the nuclei cavity size.

$$\Delta T = \frac{2T_B\sigma}{Q_{VAP}\,\rho_v\,r_c} = \frac{8\cdot10^{-4}}{r_c}$$

Here T_B is the normal boiling point, σ is the liquid/vapor surface tension, Q_{VAP} is the vaporization heat, ρ_v the vapor density in the bubble nucleus and r_c is the radius of the nucleating cavity. Since in most cases, the scattering of 0.6328 μm radiation was small, r_c could be at most about half [illegible], 0.3 μm.

Inserting this in the above expression gives an estimate of the minimum likely amount of superheating, i.e. about 25°C. This neglects the fact that the top surface of the liquid is a "nucleating surface" throughout any superheating interval. The vaporization heat absorbed there will lead to a sub-surface peaking of temperature. The lower temperatures on both sides of the sub-surface nucleating layer lead to a need for still more superheating to assure bubble growth (14).

The last sketch in Fig. 7 indicates the consequence of this superheating: when nucleation finally occurs below the surface, bubble growth occurs with explosive speed. Most (and perhaps all) of the top surface photographs are consistent with bubble growth and breakage in less than one millisecond. The dynamics of bubble growth have been analyzed in detail for the case where the bubble is immersed in an infinite liquid (15). The growth process here is considerably altered by the proximity to the free surface but one conclusion from that work appears quite pertinent here: the first few milliseconds of bubble growth are heavily influenced by inertial forces. It will be shown below that the probable thickness of the superheated layer is of the order of 100 μm for decane (less for decene). The bubble must originate in this thin layer and, as it expands, it stretches the liquid above it, thinning it considerably. Since this top layer is both thinning rapidly and vaporizing rapidly from both sides while continuing to absorb some of the incoming radiation, it is plausible that it breaks in less than a millisecond. Despite the fact that the bubble breaks quickly, it does not disappear with equal speed because of the momentum imparted to the liquid (and the weaker forces now countering the bubbles presence). The material that was above the region of nucleation is tossed up and out, frequently forming droplets that may be tossed several bubble diameters away (and out of the laser beam path). Since much of this material was superheated and its surface area per unit volume is sharply increased, there is an "explosive" release of fuel vapor that is turbulent in nature, spreading more randomly than the preceding laminar vapor plume. The impulsive downward force due to bubble expansion and subsequent vapor release causes a persisting (up to tens of milliseconds) bubble-like depression in the liquid. This movement stretches, mixes and largely erases the thermal layer previously established in the liquid over a diameter about equal to that of the bubble. This in turn largely terminates the vaporization process. Bubble collapse is induced by gravity and surface tension once the outward/downward movement of the liquid is brought to a halt. Since the laser irradiation continues (somewhat diminished by vapor absorption), the stage is set for repetition of the heat-up and bubble nucleation/growth/collapse sequence; unfortunately, the initial condition is now considerably more complex.

Repetition of this cycle feeds the gas phase with slow vaporization punctuated by rapid turbulent vapor emissions. As this vapor builds up in the gas phase it is absorbing the laser radiation and heating up. Ultimately it will ignite at some point where the proper combination of temperature plus fuel and oxygen concentration persists for a time sufficient to permit thermal runaway. Achievement of this condition is clearly dependent on the whole history of complex cycles like that just described.

Thermal Processes in the Liquid. It is of interest to attempt to assess what thermal processes dominate the heat-up time between bubble bursts. Consider first the period before the first bubble. The relative importance of heat conduction and in-depth radiation absorption is indicated by the ratio of their characteristic lengths.

$$\sqrt{K_L t}/(1/\alpha_L) = \alpha_L \sqrt{K_L t}$$

Here α_L is the absorptivity of the CO_2 laser radiation in the liquid; recall that it is about 16 cm^{-1} for decane and roughly three times higher for decene. The thermal diffusivities, K_L, of decane and decene are both about $8 \cdot 10^{-4}$ cm^2/sec (16). Then the above ratio becomes 0.45 $t^{1/2}$ for decane and 1.4 $t^{1/2}$ for decene. In all but one case (Table I), the time to the first bubble was 60 msec or less for decane so that the above ratio is typically less than about 0.1; for decene, first bubble times were 10 to 50 msec depending on radiant flux so the above ratio ranges from 0.14 to 0.3. For the high flux cases which are of primary interest here heat conduction is a minor process compared to in-depth absorption. Since the average time between successive bubbles is generally less than the time to the first bubble, this statement is generally valid at later times as well (each bubble tends to reset the clock to zero). Conduction may be important in dissipating some of the thermal energy that is mixed randomly by bubble growth/collapse. One can show also that radial conduction due to the non-uniform laser flux is unimportant in the high flux cases.

Again confining attention to the period before the first bubble, one can look at convective processes in the liquid. There are at least three sources of convective motion. First, recall the short wavelength surface waves that were mentioned briefly above as the possible result of coupling with the non-uniform laser beam profile. These build to significant amplitudes only in low flux, long delay time cases and any non-linear mixing motions that result in such cases appear to be confined to the outer periphery of the beam profile. There is also some small in/out radial convective motion associated with the oscillation induced by the photon-pressure and laminar vapor plume. One can estimate that the fundamental frequency of this oscillation should be about 30 Hertz (6) so it is generally slow and probably of minimal effect in high flux ignition cases.

There are two other sources of convective motion prior to the first bubble-buoyant flow and surface tension gradient flow (17). The buoyant flow is a result of the non-one-dimensional heating of the top of the liquid. Here we follow ref. 17 but note that in the present case inertial forces are more significant than viscous forces in balancing the buoyancy force. Consider a radial flow proceeding upward and then outward from the center of the laser beam impact point. From a steady state balance of buoyancy and fluid inertia one gets the following (the steady state balance is an upper limit on the present dynamic case).

$$\rho_L v_B \frac{dv_B}{dx} = \beta_L g \Delta T$$

$$\rho_L \frac{v_B^2}{R_L} = \beta_L g (T_B - T_\infty)$$

so

$$v_B = \left[\frac{R_L}{\rho_L} \beta_L g (T_B - T_\infty)\right]^{1/2}$$

Here v_B is the buoyantly induced flow velocity, ρL is the liquid density, β_L is the change of density with temperature, and T_B is the liquid boiling point. The use of R_L, the laser beam radius, as the characteristic length in the upward flow is rough so we can only estimate v_B crudely. Inserting typical numbers for decane (about the same as decene) one finds v_B = 8 cm/sec. Recall that this is a steady state upper limit so that, roughly, the average transient value acting on events over a time scale of (R_L/v_B) = 40 msec is about half this or 4 cm/sec. Then only for bubble delay times of the order of 10 msec is this motion small; for delays of the order of 100 msec it is substantial, causing a full replacement of the liquid beneath the beam profile.

Consider next the flow driven by the surface tension gradient that is a consequence of the non-uniform laser beam profile. The steady state balance is now between the surface tension gradient force and the inertia of the radial outward flow. Roughly, for unit volume of liquid, undergoing this radial motion we have

$$\rho_L \frac{v_s^2}{R_L} = \left(\frac{\partial\sigma}{\partial T}\right) \Delta T \quad 2\pi R_L$$

or

$$v_s = \left[\frac{1}{\rho_L} \left(\frac{\partial\sigma}{\partial T}\right) \left(T_B - T_\infty\right) 2\pi R_L^2\right]^{1/2}$$

Here $(\partial\sigma/\partial T)$ is the change in surface tension with temperature; the other symbols are the same as before. Inserting typical values for decane (decene is again similar), one finds v_s = 3 cm/sec. Again this is the steady state upper limit so, roughly, half this value is that pertinent to our transient heat-up process. Since this flow is in the same direction as the buoyant flow, this result provides a small reinforcement to the previous conclusion that these fluid motions become appreciable on a time scale of about 100 msec and are small perturbations on a 10 msec time scale.

This conclusion is reinforced by the experimental behavior of a piece of foam plastic placed on the liquid surface about 1 cm away from the irradiated area in several early high flux tests. This object was always pushed to the side of the container during a 2-3 sec. laser irradition but its rate of movement was negligible during the time sequence of interest here.

Again, since the main concern here is high flux short delay behavior, we can assume for now that the above fluid motions are not significant. Then in the period before the first bubble the dominant energy transport mode is in-depth radiation absorption which follows Beer's law. In this case is quite simple (1).

$$T_s = T_\infty + \left[\frac{(1-r_L)\ F\ \alpha_L}{\rho_L C_L}\right] t$$

Here α_L is the effective absorptivity (corrected for angle of radiation impingement; note that F and α_L have equal and opposite corrections for incident angle which therefore cancel out), r_L is surface reflectivity (generally about 5%) and C_L is the liquid heat capacity. This expression, if solved for time, does give approximately correct values of times to reach the surface depression caused by the start of significant vaporization (roughly, at the boiling point). The temperature distribution is simply

$$T(x) = T_\infty + (T_s - T_\infty)\ e^{-\alpha_L x}$$

Since we already have an estimate of the extent of superheating prior to the first bubble (~25°C) we can use this distribution to calculate the depth of the layer above the boiling point; this is the origin of the 100 micron superheat thickness for decane quoted previously. It will be about 1/3 this value for decene; this implies that the bubble size will also be reduced by about this factor, which is consistent with Table I. Recall again that this distribution does not account for loss of heat from the top surface by laminar vaporization so it becomes increasingly approximate as such a process evolves.

Once the first bubble grows and bursts, we immediately have a new form of convective motion in the liquid. As was noted previously, the initial motion induced by the bubble is largely that of radial expansion but it quickly becomes more complex because of the surface proximity. Some of the schlieren pictures appear to indicate that the net short term effect of the bubble is to push a segment of the upper thermal layer (about equal in diameter to the bubble in width and one to two diameters deep) down into the cold bulk of the fluid; this is qualitatively consistent with other observations on nucleate boiling (18). The impact of this depends on the product of flux level and liquid absorptivity (see equation above). If the product is high (as in the high flux decene case of Table I), the result, already mentioned, is a second bubble in the bottom (or side) of the first, despite any convective/conductive cooling this fluid may have experienced during the growth of the original bubble. The further result is quite complex mixing motion in the liquid that should lead to erratic high frequency bubbles.

If the product $(\alpha_L \cdot F)$ is low (as in the low flux decane case of Table I), the bubble will collapse and at least partially mix a layer of the order one to two times its original diameter. The mixing, if total, would fully reset the heating process to zero and another bubble would not follow until a time dictated by the above radiation-dominated equation (solved with $T_S \geq T_{BOIL}$); residual sub-surface convection due to bubble collapse would lengthen the interval. This behavior for the small $(\alpha_L \cdot F)$ case would imply a bubble interval comparable to the delay time to the first bubble. This behavior is only roughly what one sees for decane at low fluxes, as indicated by Table I. The shorter interval between bubbles after

the first implies that the bubble-induced mixing is only partial and heat from the previous cycle makes a contribution to shortening the next one. (This is countered by increasing absorption of the laser radiation passing through the accumulating vapor in the gas phase.)

Coupling to the Gas Phase. These bubble-induced liquid motions complicate the determination of bubble frequency considerably. This frequency is of interest because it is probable that it is half the key to the rate of fuel vaporization; the other half of the key is the amount of fuel vaporized in the bubble growth/burst/collapse sequence (plus any vaporization between bubbles). Although one could speculate on the factors affecting this vaporization rate, it is best to attempt direct measurements (a future experiment).

For now, we note only that there are three idealized limiting cases of vaporization behavior that facilitate analysis of the gas phase vapor build-up. In all cases the vapor is absorbing some of the laser beam, further complicating the gas-liquid coupling. The first is the purely laminar vaporization case in which a bubble never occurs (or, if it does, the bubble size is small compared to all other characteristic lengths in the problem). The present ignition processes begin this way but quickly get more complex. Such relatively simple behavior has been observed with solid fuel ignition by radiation (1,19). This behavior is favored by high condensed phase viscosity and absorptivity. Since the plume here is fairly mono-directional its interaction with the laser beam depends strongly on the incident angle of the beam; such behavior has been seen experimentally (5). One can anticipate a substantial beam diameter effect as well. Fuel vapor/air mixing would be slow also.

The second limiting case is that of very low frequency bubbling as described above for the liquid. To the gas this presents a sequence of widely-spaced vapor pulses that might be approximated by delta functions. Transport in the gas is convective and increasingly turbulent; the bursting bubbles generate a non-directional vapor plume and between bursts, the negative buoyancy of heavy fuel vapors forces them down, spreading them out away from the incident beam.

The third limiting case corresponds to high frequency, large bubble bursts as described above for the liquid. To the gas this presents a nearly constant, non-directional turbulent vapor source. One would expect a more or less hemispherical envelope of vapor to accumulate over the region where the beam is incident. Since the gradients would be primarily radial, the interaction with the laser beam becomes nearly independent of its incident angle; this trend at high fluxes is also seen experimentally (5). There is a beam size effect if the beam becomes larger than the turbulent vapor diffusion length in the gas phase. This is because a large diameter beam means simultaneous bubbling will occur over a large liquid surface area; there will be many bubbles within the beam diameter. In the limit of a large ratio, the gas phase behavior becomes one-dimensional and an incident beam angle dependence is reintroduced.

These limiting cases are more amenable to at least approximate analysis. The general behavior seen in the present experiments tends to fall between the second and third limits described above.

Observing the Conditions that Produce Ignition. So far the main emphasis of this study has been on the observation of the liquid behavior during the ignition period. However, more observations of the gas phase, especially quantitative concentration and temperature measurements, are necessary to understand the ignition mechanism and to develop theoretical models. To get at these gas phase properties we have undertaken a feasibility study of the use of holographic interferometry. Since refractive index is a function of species concentration and temperature, two different wavelengths need to be used to obtain both quantities. Similar measurements were attempted previously; one with a two wavelength holographic interferometer for a steady state flame study (20) and the other with a two wavelength interferometer for a time dependent ignition study of a solid (19). In this study, a two wavelength holographic interferometer will be used since it provides phase information without imposing requirements of very high quality on the optical components. As a first step, a single wavelength holographic interferometry system has been set up to assess the technique. The system is illustrated in Figure 8. An additional wavelength from an Ar-ion laser will be added to this system in the near future. A preliminary result from the system in Fig. 8 is shown in Figure 9. This picture was taken by the "double exposure technique" in which the hologram was constructed by taking two exposures: before the CO_2 laser irradiation as a base case and then during the CO_2 laser irradiation. At present, the timing between the start of laser irradiation and the picture taking is not fixed precisely and the exact time of Figure 9 relative to the start of the laser irradiation is not known. Figure 9 shows the fine details of the liquid behavior and the potential to obtain quantitative information in the gas phase. High speed pictures of such transient holograms will be attempted in the near future.

4. Concluding Remarks

The sequence of events that leads to liquid fuel ignition during high flux irradiation is increasingly clear. Supersaturation and sub-surface bubble nucleation add semi-periodic disruptions to what would otherwise be a laminar vaporization process such as that seen in solids. Even the laminar case is quite complex, especially because radiation absorption by the fuel vapors adds further coupling between condensed phase and gas phase behavior. In general, the irregular liquid and gas phase mixing motions that result from growth and bursting of bubbles make the ignition process stochastic in nature. Since ignition in the gas requires just the right combination of fuel, oxygen and temperature and this is achieved in a field dominated by large-scale turbulence, ignition delay cannot be precisely repeatable. There are, however, clear trends of behavior with increasing flux or fuel absorptivity (increases in either accelerate the whole sequence of events, lead to a dominance of bubbling phenomena and decrease the ignition delay) and we have rationalized them qualitatively. There is a need now to quantify the fuel vaporization rate and the precise conditions in the gas that lead to ignition. There will then be a firm basis for constructing and testing at least limiting behavior models of the ignition process.

5. Acknowledgments

This work is supported by the Air Force Office of Scientific Research under Contract AFOSR-ISSA-80-00010. The authors would like to thank Mr. William H. Wooden for his assistance in conducting experiments.

6. Reference

1. Ohlemiller, T. J., and Summerfield, M., "Radiative Ignition of Polymeric Materials in Oxygen/Nitrogen Mixtures," Thirteenth Symposium (International) on Combustion, Combustion Institute, 1971, pp. 1087-1094.

2. Stegman, R. L., Schriempf, J. T., and Hettche, L. R., "Experimental Studies of Laser-Supported Absorption Waves with 5 ms Pulses of 10.6μ Radiation," J. Appl. Phys., Vol. 44, 1973, pp. 3675-3681.

3. Chien, K. Y., "Vaporization of Liquid-Air Droplets by High-Power Laser Beams," AIAA J., 1975, pp. 1647-1652.

4. Emmony, D. C., "High Speed Study of Laser-Liquid Interaction," J. Photo. Sci., 1977, pp. 41-44.

5. Kashiwagi, T., "Ignition of a Liquid Fuel Under High Intensity Radiation." Comb. Sci. Tech., Vol. 21, 1980, pp. 131-139.

6. Kashiwagi, T., Baum, H. R., and Rockett, J. A., "Ignition of a Liquid Fuel Under High Intensity Radiation," AFOSR-TR-80-0476, 1980.

7. Selected Infrared Spectral Data, American Petroleum Institute Research Project 44, Vol. 3, Texas A & M University, 1977.

8. Weast, R. C. (ed.), Handbook of Chemistry and Physics, The Chemical Rubber Company, 1969.

9. Handbook of Tables for Applied Engineering Science, CRC Press, Cleveland, Ohio, 1973, p. 388.

10. Blander, M., and Katz, J. L., "Bubble Nucleation in Liquids," AIChE J., Vol. 21, 1975, pp. 833-848.

11. Reid, R. C., "Superheated Liquids," American Scientist, Vol. 64, 1976, pp. 146-156.

12. Porteous, W., and Blander, M., "Limits of Superheat and Explosive Boiling of Light Hydrocarbons, Halocarbons, and Hydrocarbon Mixtures," AIChE J., Vol. 21, 1975, pp. 560-566.

13. Hsu, Y. Y., and Graham, R. W., Transport Processes in Boiling and Two-Phase Systems, McGraw-Hill Book Co. 1976, p. 6.

14. Ibid, p. 7.

15. Ibid, p. 18.

16. Chemical Engineers' Handbook edited by J. H. Perry, McGraw-Hill Book Co., 1950, p. 459.

17. Murad, R. J., Lamendola, J., Isoda, H., and Summerfield, M., "A Study of Some Factors Influencing the Ignition of a Liquid Fuel Pool." Comb. Flame, Vol. 15, 1970, pp. 289-298.

18. Hsu, Y. Y., and Graham, R. W., op. cit., p. 14.

19. Mutoh, N., Hirano, T. and Akita, K., "Experimental Study of Radiative Ignition of Polymethylmethacrylate." Seventeenth Symposium (International) on Combustion, The Combustion Institute, 1978, pp. 1183-1190.

20. Mayinger, F., and Panknin, W., "Holographic Two-Wavelength Interferometry for Measurement of Combined Heat and Mass Transfer." Combustion Measurements, edited by R. Goulard, Academic Press, 1976, pp. 270-283.

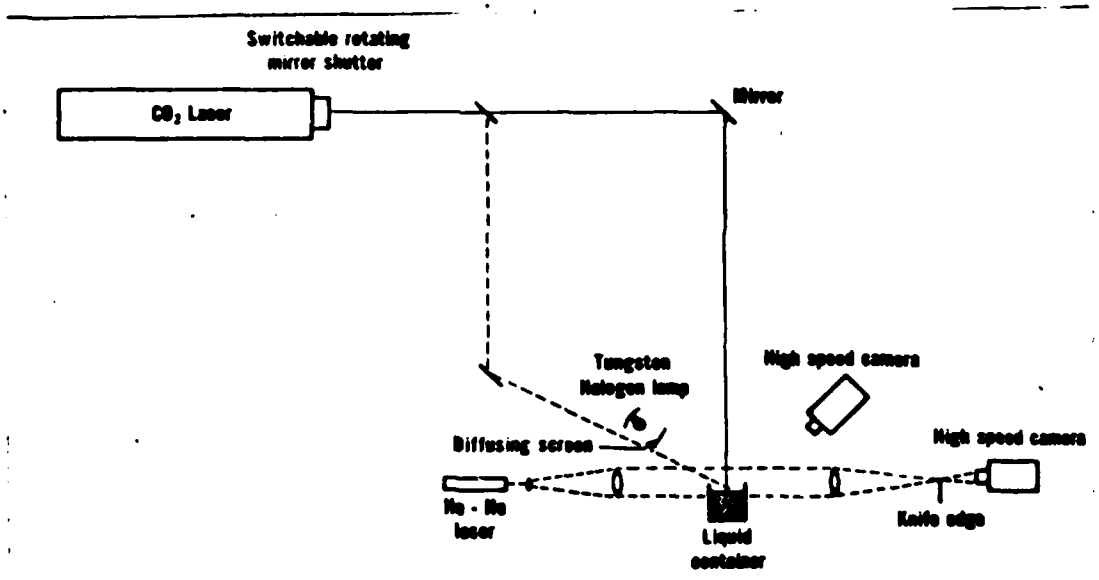

1. Schematic illustration of experimental apparatus.

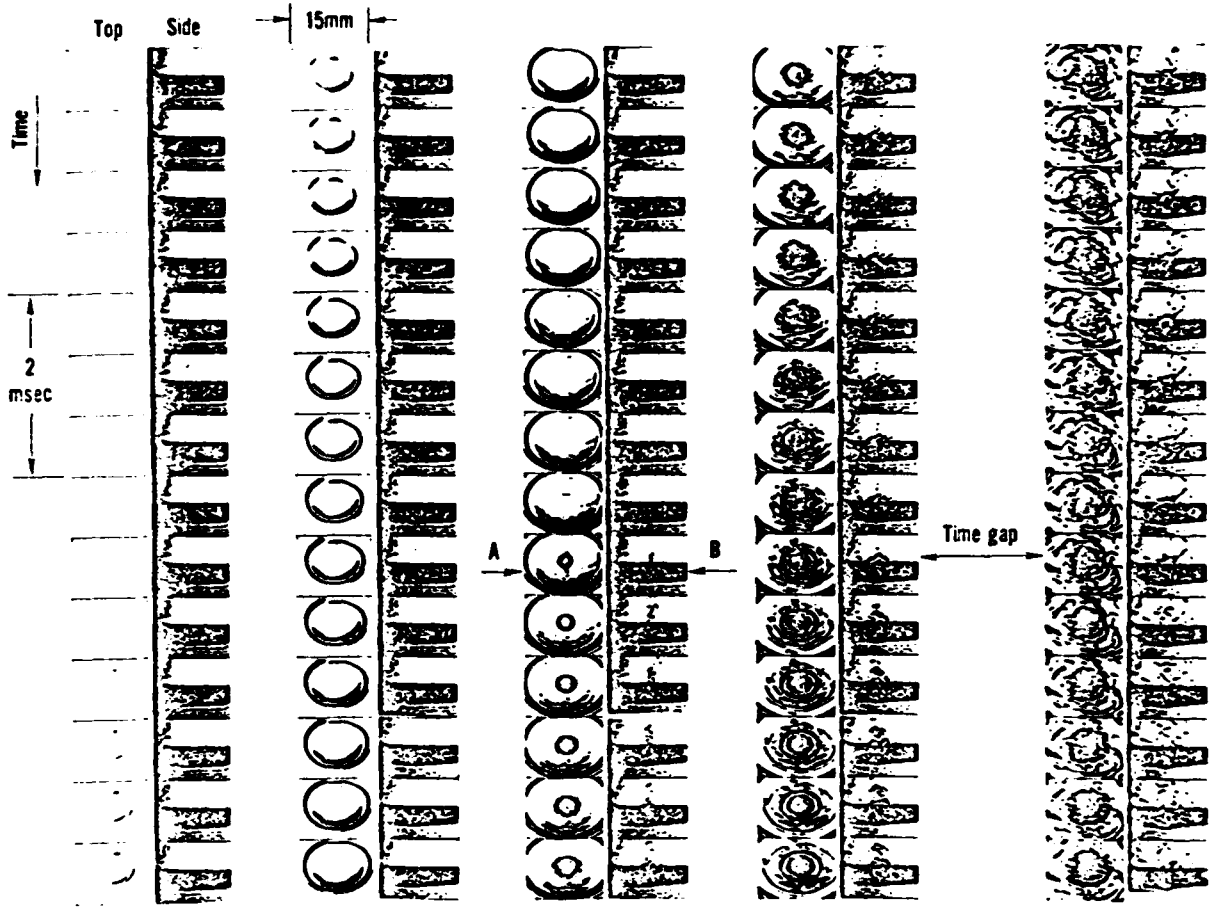

Top view direct picture and side view schlieren picture; left columns, top view; right columns, side view. Decane, laser flux of 740 W/cm^2, incident laser angle of 30°. A: appearance of hole due to first bubble in top view; B: corresponding sudden release of liquid vapor. Time gap: about 30 msec.

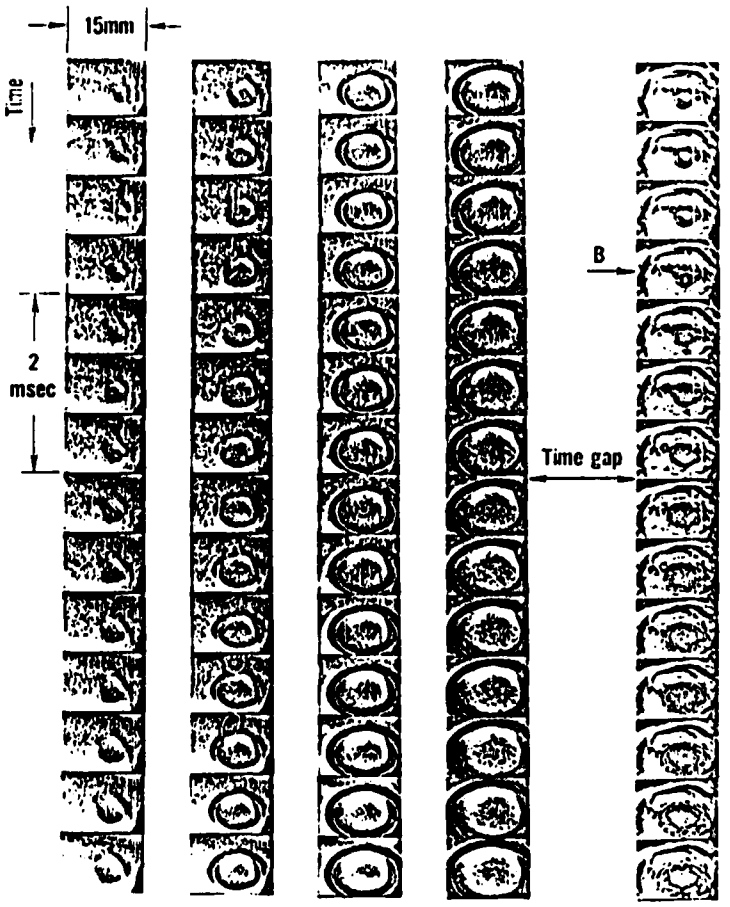

3a. Top view picture, decane, laser flux of 410 W/cm^2 and incident laser angle of 30°.
B: appearance of hole due to first bubble
Time gap: about 350 msec

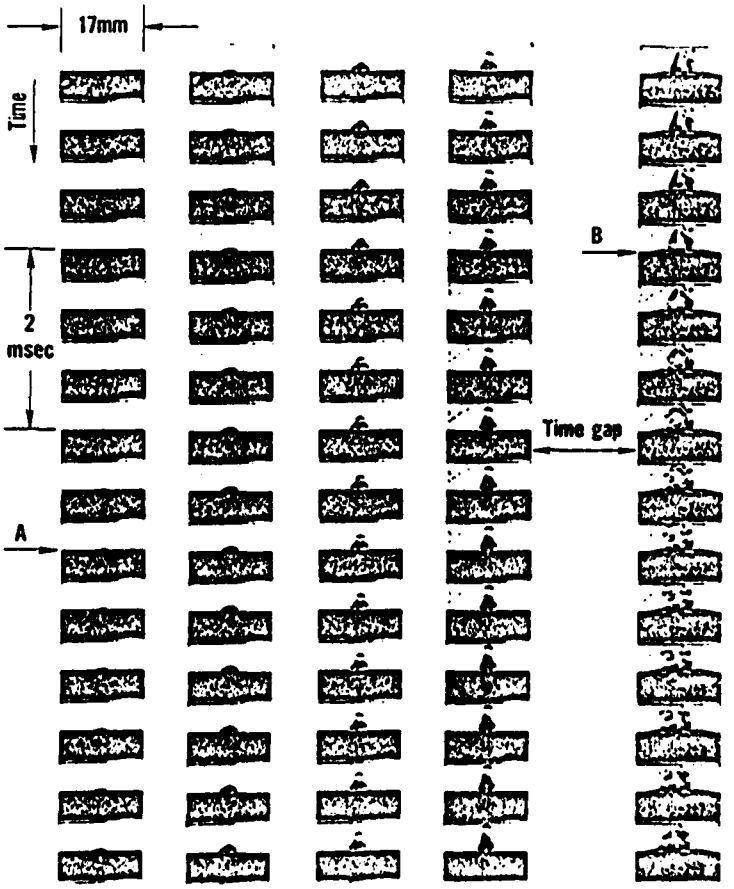

3b. Side view schlieren picture, same test as Fig. 3a.
A: appearance of laminar vapor plume.
B: sudden release of liquid vapor by bubbl burst

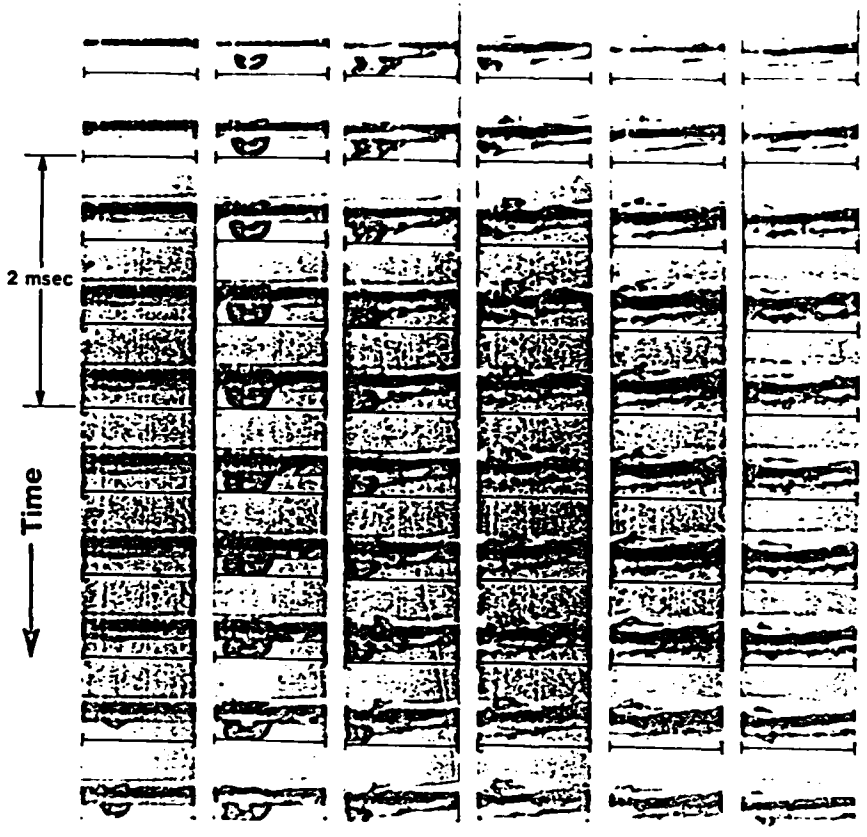

Side view closeup direct picture near the decane surface, laser flux of about 2500 W/cm^2 with incident laser angle of 30° from right to left.

Fig 4

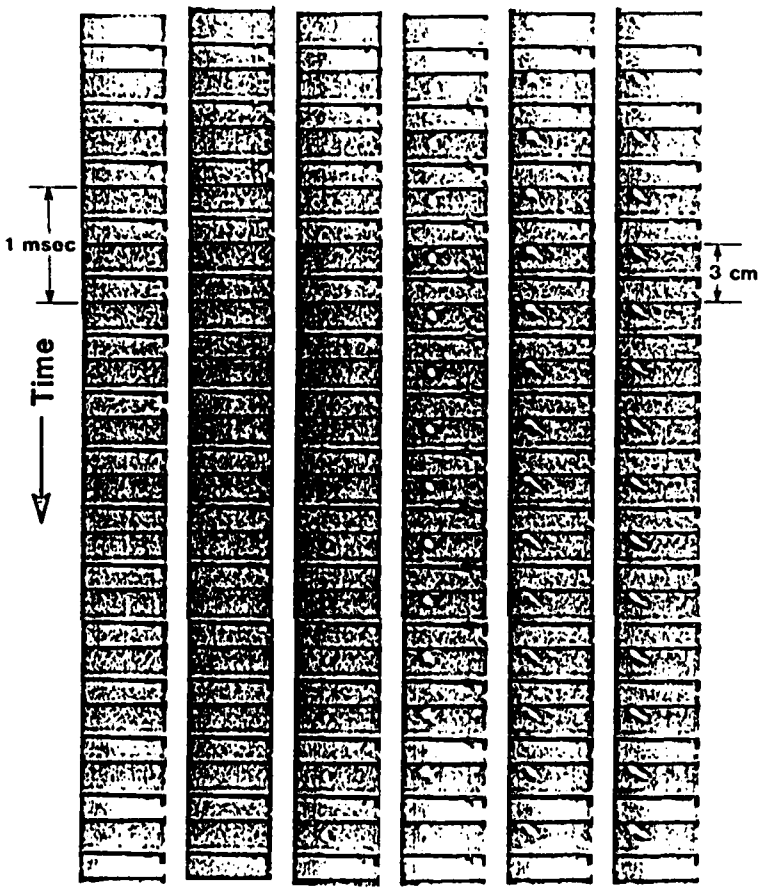

Side view direct picture to observe the location of the first appearance of flame. Decane at a laser flux of about 2500 W/cm^2 with incident laser angle of 30° from left to right.

Fig. 5

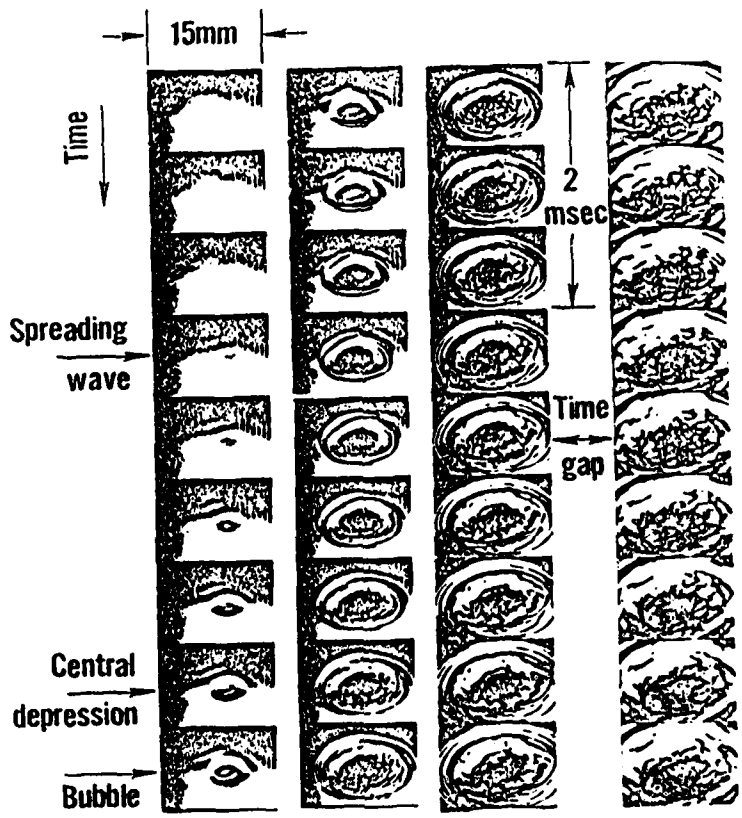

6. Top view picture of decene with laser flux o 910 W/cm^2 and incident laser angle of 90°. Time gap is about 18 msec.

Fig. 6

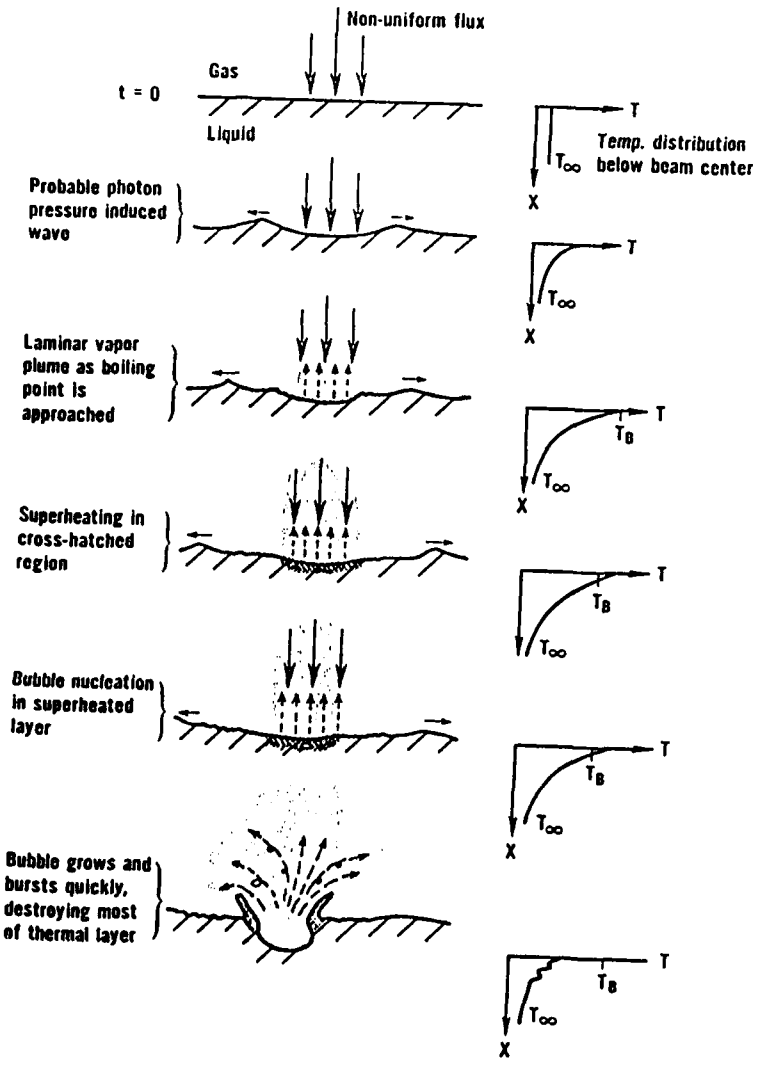

7. Idealized sequence of bubble development; the sequence repeats but the starting condition i no longer as simple as that in the first sket

Fig. 1

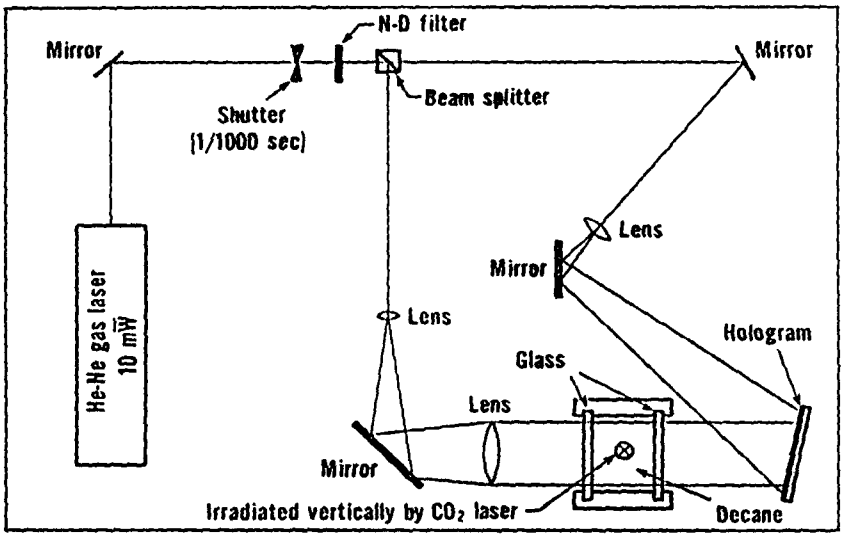

8. Schematic illustration of holographic interferometry set up.

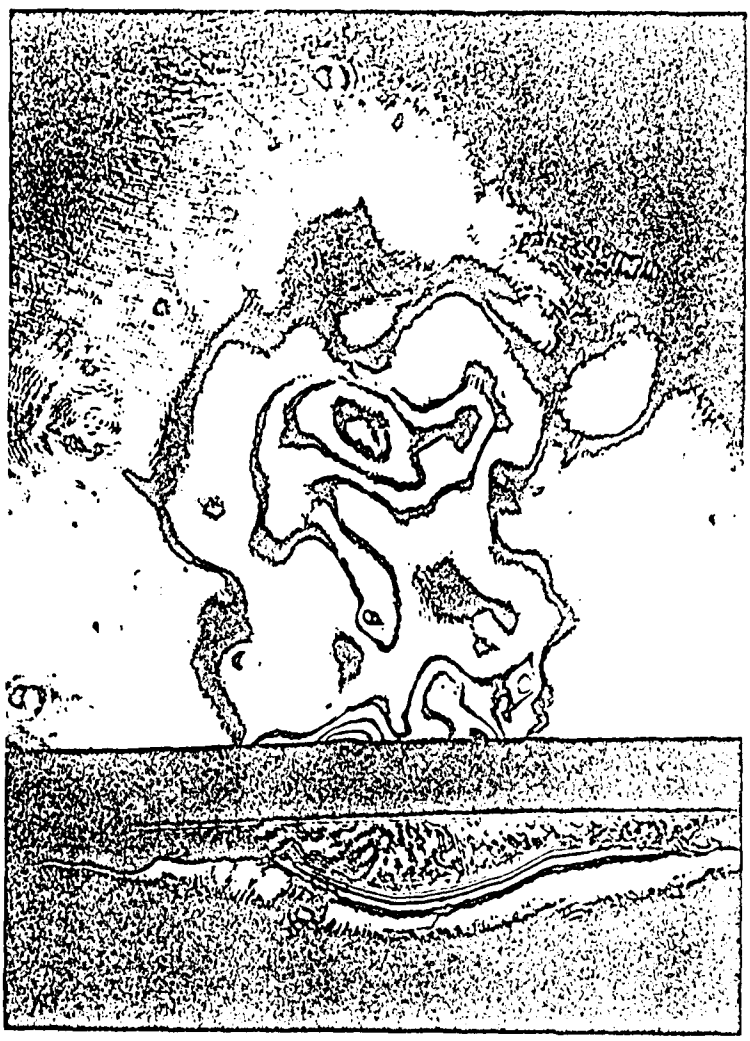

9. Preliminary result from set-up in Fig. 8. Decane with laser flux of 435 W/cm^2 and incid laser angle of 90°. Phase contours correspon to density contours.

TABLE I VARIOUS TIMES OF EVENTS AFTER LASER IRRADIATION

Liquid	Total Laser Power (W)	Laser Peak Flux (W/cm^2)	θ (degree)	t_1 (msec)	t_2 (msec)	Δt (msec)	t_{ign} (msec)	d (mm)
Decane	340	910	90°	17	20～30	12～17	350 ～ 360	～3
Decane	340	730	30°	23	24～26	9～13	1000～1400	～3
Decane	200	435	90°	-	57～64	20～37	No Ignition	～2.5
Decane	200	410	30°	-	60～360	66～87	No Ignition	～3
Decene	340	910	90°	4～6	7～10	～8	39 ～ 46	-
Decene	340	730	30°	8～10	23～31	-	46 ～ 51	-
Decene	200	435	90°	～11	46	-	63 ～ 69	～0.8
Decene	200	410	30°	17～21	47～55	9～11	81 ～ 84	～1

θ: incident laser angle

t_1: time to appearance of central depression

t_2: time to appearance of first bubble

Δt: period between bubbles

t_{ign}: ignition delay time

d: diameter of bubble

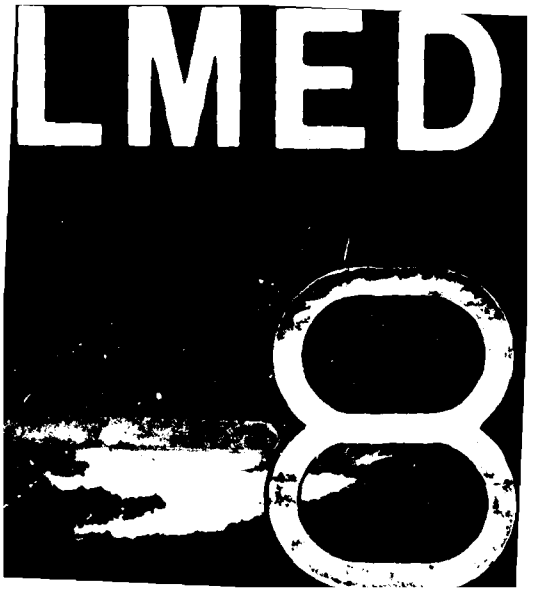
LMED
8